PCA-SVM

张宏杰[1]，　侯妍妍[2]

(1.　　　　　　　　　　　　　　　300160; 2.　　　　　　　　　　　　　　　　050031)

：　　　　　　　　　　　　　　　，

　　　　　　，　　　　　　　　　9

　　　．　　　　　　　　　　　，　　PCA(

)　　　　SVM(　　　)　　　，　　PCA

　　　　　，　　　　　　，

PCA-SVM　　　　SVM　　　，　　SVM　　　．

：　　　；　　　；　　　；

张宏杰

0　序　言

　　　　　、

　，　　　，

　　，　．　　　　、

　　，　　　　、　　　、

　、

　　　　　[1－5]．

　(　　　　、　　　)

　，　　　　，

　　　、　　　、　　　，

　　．

，

，

$$S = \frac{1}{m}\sum_{i=1}^{n} - (z_i - \mu)(z_i - \mu)^{\mathrm{T}} \qquad (1)$$

n　　　　　　$z_i(i = 1, 2 \cdots n)$,

：$\mu = \frac{1}{m}\sum_{i=1}^{n} z_i$．　S　　　　　，　k

$(k \leqslant n)$　　　　　　　　　　k

$$\theta = \sum_{i=1}^{k} \lambda_i / \sum_{i=1}^{n} \lambda_i \qquad (2)$$

：λ_i　S　　　　　．

$Z = Z + Z, \qquad Z = V_k P, V_k = [\nu_1, \nu_2 \cdots \nu_k]$

，$\nu_i(i = 1, 2 \cdots k)$　　　　λ_i

　　　　；P　　　；Z　Z

　．　k　　　　　　PCA

Z　　　　　　，　　　$Z^n \to Z^k$　　．

1　PCA-SVM 方法

　　　　，　　　，

　　　，　　　　[6]

$$\min\left\{\frac{1}{2}\|W^2\| + C\sum(\zeta_i + \zeta_i^*)\right\} \qquad (3)$$

：W　　　　　　，$W \in R^n$;　　C

$\varepsilon($　　　　　　　)

，　　　　；ζ_i, ζ_i^*　　　，

　　　　　．

[7]，

(3)

$$y_i - (Wx_i) - b \leqslant \varepsilon + \zeta_i$$
$$(Wx_i) + b - y_i \leqslant \varepsilon + \zeta_i^* \quad (i = 1, 2 \cdots n)$$
$$\zeta_i, \zeta_i^* \geqslant 0 \tag{4}$$

: x_i, y_i 　　 n 　　　　　 ; $b \in R$ 　　　 . 　(3)

　　　　　　 , 　　　　　　 ,

(5)　　 , 　　　　　　 α_i, α_i^*

(6), 　　　　　　　 (7),

$$\sum_{i=1}^{n} (\alpha_i - \alpha_i^*) = 0$$
$$0 \leqslant \alpha_i, \alpha_i^* \leqslant C, \ i = 1, 2 \cdots n \tag{5}$$

$$W(\alpha_i, \alpha_i^*) = -\varepsilon \sum_{i=1}^{n} (\alpha_i + \alpha_i^*) + \frac{1}{2} \sum_{i=1}^{n} y_i (\alpha_i^* - \alpha_i) -$$
$$\frac{1}{2} \sum_{i,j=1}^{n} (\alpha_i^* - \alpha_i)(\alpha_j^* - \alpha_j)(xx_i) \tag{6}$$

$$f[\phi(x)] = \sum (\alpha_i^* - \alpha_i)(xx_i) + b \tag{7}$$

(7)

　　 $K(x, x_i)$ 　　　　　　　 .

(8)　 SVM 　　　　　 ,

$$f[\phi(x)] = \sum (\alpha_i^* - \alpha_i) K(xx_i) + b \tag{8}$$

SVM 　　　　　　　　 、Sigmoid

、　　　　　　 , 　　　　　

　　　 , 　(9) 　 .

$$K(x, x_i) = \exp\left(-\frac{\| x - x_i \|^2}{r^2}\right) \tag{9}$$

: r 　　　　 , 　　　　　 .

2 电极位移信号的特征提取

　　 、　　　 、　　　　 、A/D 　　　 .
0.7 mm 　　　　　　　　 ,
2.0 kN, 　　　　　　 6 mm,
3.2 ~4.4 kA 　 , 　60 　　　 ,
　　　 , 　　 MPa. 　1
4.4 kA, 　　　 20 　　　　　 、
　　　 ,

　　 , 　　　　　　　 ,
　　　　 [8] .

　　 1b 　　　　　　　 ,
、　　　　　　 , 　2
　　 , 　1b 　d
(　1a 　b 　　　),

图 1

Fig. 1 Original signal of dynamic resistance and electrode displacement

　　　　　　　　 . 　1b 　e
　　 .
　　　 , 　　　　 ,
　　 (f 　　　),
　　 , 　　 .
　　　　　　　　　 ,
9
, 　λ_1 　　　　　 (　　　 /
　); D_1 　　　　 ,
　　　　 ; D_2 　　　　　
　　　 ; D_3 　　　　　　 ; D_4
　　　 ; ΔD 　　　　　 ,
　　　　 ; v_1
　　 ,
(　1b 　d 　) 　　　　　 ;
v_2 　　　　　　　 ,
(　1b 　d 　e 　　)
　　　　　 , 　　　 ,
　　　　　　 ; v_3
　　　 (　1b 　e 　f
) 　　　 .
　　 .
　　 2 　　　 60 　　
　　 .

3 PCA-SVM 焊点接头强度预测

图 2

Fig. 2　Scatter diagrams for characteristic value of electrode displacement

，　　　　　　　PCA-SVM　　　　　　　，　　　　　　　　　，

，　　　　　　　　，　　　　　　　　，

．　　　　　．　　　　　　　　．

，　　　　　　　1　　　　　　　．

．　　　PCA　，　　4　　　　　　1　4

0.347 8,0.013 1,0.009 8,0.004,　　　　(60×4　　　　　)

91.895 2%,95.369 6%,97.967 9%,　　　　，　　　　　　，

99.033%,　　　　　85%,　5　9　　　　　　PCA-SVM　　　　　．

，　　　　　　PCA-SVM　　　　　，

SVM

60×9

表 1

Table 1　Results of PCA method

	λ_i	θ(%)	α(%)
1	0.347 8	91.895 2	91.895 2
2	0.013 1	3.474 4	95.369 6
3	0.009 8	2.600 1	97.969 7
4	0.004	1.063 3	99.033
5	0.001 9	0.490 8	99.523 8
6	0.001	0.252 6	99.776 4
7	0.000 7	0.185 2	99.961 6
8	0.000 1	0.033 4	99.995
9	0.000 02	0.005	100

（　　　　　　　　　　　　　r,

　　　　　　　）、　　　　　ε

C（　　　　　　　　　　　）

[8]．C　，ε　　，　　　　　，　　　，

，　　　　　　　；C　　，ε

，　　　　，　　　，

．

[4]

：

、　　　　　、　　　　.
　　　　　　　　，　　　　　　r
0. 89,　　　　　　　　1 000　0.001
　　　.
　　3　　　　　　　　，　2
　　　　　　　　，　　　　PCA-SVM
　　　　　.

(a) SVM预测结果

(b) PCA-SVM预测结果
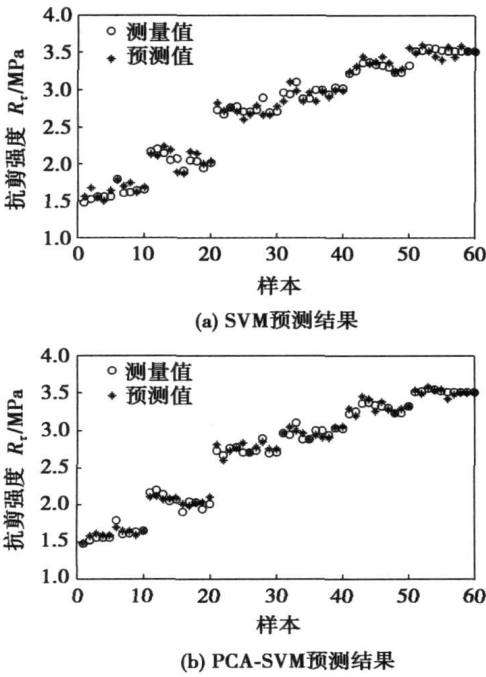
图 3　PCA-SVM 与 SVM

Fig. 3　Tensile- shear strength prediction results of welded spot
joint with SVM and PCA-SVM method

表 2　PCA-SVM 与 SVM

Table 2　Prediction error of shear strength of welded spot joint

	$e_{min}(\%)$	$e_{max}(\%)$	$e_1(\%)$	$e_2(\%)$
SVM	0.02	10. 43	3.99	4. 80
PCA-SVM	0.02	5. 5	1.95	2. 42

4　结　　论

（1）　　　SVM　　PCA-SVM
　　　　　　　　　　　　　，
　　　　　　　　　　、
　　　　　　　　　.

（2）　PCA　　　　　　　SVM
　，　　PCA
　　　　，
　　　　　　　，
　　　，　　PCA　　SVM　　　　　SVM
　，　　　SVM　　　　　.

　　　　　:

[1]　Hao M, Osman K A. Development in characterization of resistance
　　　spot welding of aluminum[J] . Welding Journal, 1996, 75(1) : 1— 8.
[2]　Cho Y, Kim Y, Rhee S, et al. Development of a quality estimation
　　　model using multivariate analysis during resistance spot welding[J] .
　　　Proceedings of the Institution of Mechanical Engineers, 2001, 215
　　　(11) : 1529— 1538.
[3]　Cho , Rhee S, Kim Y, et al. Experimental study of nugget formation
　　　in resistance spot welding[J] . Welding Journal, 2003, 4(13) : 195—
　　　200.
[4]　Javed M A, Sanders S A. Neural networks based learning and adaptive
　　　control for manufacturing system[J] . IEEE Intelligence for Mechanical
　　　System Proceeding IROS'91, 1991, 11(3) : 242— 246.
[5]　Brown J D, Rodd M G, Willams N T, et al. Application of artificial
　　　intelligence techniques to resistance spot welds[J] . Ironmaking and
　　　Steelmaking, 1998, 25(3) : 199— 204.
[6]　　　　　　，　　　　. 　　　　　　　　　　[M] . 　　 :
　　　　，1990.
[7]　Vladimir N, Vapnik. The nature of statistical learning theory[M] .
　　　　　　，　. 　 : 　　　　　　　，1999.
[8]　Garza F J, Das M. Identification of time-varying resistance during
　　　welding[J] . IEEE Instrumentation and Measurement Technology,
　　　2000, 5(3) : 1534— 1539.

　　　　　:　　　，　，1977　　　　，　　　，　　　，　.
　　　　　　　.　　　　9　.

Email：starbeifeng@163.com

(State Key Laboratory of Advanced Welding Production Technology, Harbin Institute of Technology, Harbin 150001, China). p93—96

Abstract:　Tensile strength, bending strength, impact toughness and non-destructive inspection tests of TIG welded 20G/316L clad pipe joint were carried out. The microstructure and the diffusion of the major alloying elements were analysed using optical microscopy, SEM and chemical analysis. The results showed that the weld can be divided into four layers including carbon steel layer, diffusion layer, transition layer and stainless steel layer. The microstructure in diffusion layer was characterized by the martensite and retained austenite. The transition layer only contained austenite, and the stainless steel layer included afterbirth-like crystal. The defect-free joint was produced and performed well under the experimental parameters. The concentration of nickel and chromium element in weld root did not decrease compared with the corresponding welding materials, which proved that the employment of transition welding wire could maintain the concentration of the major alloying elements in welding root.

Key words:　20G/316L clad pipe; TIG; microstructure; mechanical properties

Quality evaluation of the resistance spot welding based on PCA-SVM

ZHANG Hongjie[1], HOU Yanyan[2] (1. School of Machinery and Electron, Tianjin Polytechnic University, Tianjin 300160, China; 2. Department of Architecture Engineering, Hebei College of Administration, Shijiazhuang 050031, China). p97—100

Abstract:　The electrode displacement and dynamic resistance signals of resistance spot welding process are collected synchronously. Through the time-domain analysis of electrode displacement signal in the welding process, nine characteristic parameters relating to weld quality are picked up to set up a set of data which characterizes the input samples, on the basis of the different phase of nugget forming marked by simultaneous dynamic resistance signal. The principal component analysis (PCA) to remove the self-correlation of input characteristics and realize dimensionality reduction is integrated with the conventional method of support vector machine(SVM), while the shear strength of welded spot was taken as the evaluation index of welded spot quality. The comparison of predicted results under PCA-SVM and conventional SVM by means of cross-validation test shows that PCA-SVM algorithm improves the generalization ability and the predicted accuracy of SVM method.

Key words:　resistance spot welding; principal component analysis; support vector machine; regression analysis

Numerical simulation of the temperature field during resistance spot welding with rectangular electrode

ZHANG Xiaoqi[1,2], XU Guocheng[1], WANG Chunsheng[1,3], WEN Jing[1] (1. School of Material Science and Engineering, Jilin University, Changchun 130025, China; 2. Jilin Teachers Institute of Engineeriy and Fechnology, Changchen 130052, China; 3. Changchun Railway Vehicles Corporation, Changchun 130062, China). p101—104

Abstract:　The temperature field during resistance spot welding with rectangular electrode was simulated using ANSYS. The physical model was properly simplified on the basis of simulation accuracy and technological conditions. One-quarter three-dimensional finite element model during resistance spot welding was built in which the contact resistance was substituted by the electric resistivity. The results show that at the beginning of welding, the edge of electrodes has the highest temperature because of high stress induced by the electrode force. As welding time is longer, the contact resistance decreases and the highest temperature position moves to inside, the nugget appears to be similar with the conventional spot welding.

Key words:　rectangular electrode; numerical simulation; temperature field

Laser-based visual recognition of multi-pass seam in robot arc welding

ZHANG Huajun[1,2], ZHANG Guangjun[1], CAI Chunbo[2], GAO Hongming[1], WU Lin[1] (1. State Key Laboratory of Advanced Welding Production Technology, Harbin Institute of Technology, Harbin 150001, China; 2. College of Material Science and Engineering, Harbin University of Science and Technology, Harbin 150040, China). p105—108

Abstract:　It is very necessary for the improvement of weld quality and the realization of robot automatic production to detect multi-pass weld profile parameters automatically. Automatic detective system of multi-pass weld profile parameters by band laser visual sensor was developed. The procedure of image process is as follows: smoothing, center recognition by longitudinal grey gradient, twice slope smooth process, and multiple peaks search by laser seam image analysis. It is very important for seam tracking, arc length control and torch attitude adjustment to obtain four character points of weld seam profile. And the recognition results agree with the experimental results.

Key words:　multipass welding; laser visual sensor; image process; twice slope smooth process; robot arc welding

Research on gravity compensation algorithm for tool-assembling with force control in remote welding

WEI Xiuquan, WU Lin, GAO Hongming, LI Haichao (State Key Laboratory of Advanced Welding Production Technology, Harbin Institute of Technology, Harbin 150001, China). p109—112

Abstract:　Based on the control strategy of global teleoperative and local autonomous, a tool-assembling experimental system with force control for remote welding is established. The tool gravity calculation and linear least-squares algorithm are adopted to calibrate the tool load parameter, and a tool gravity compensation algorithm based on the tool load parameter vector is proposed to eliminate the gravity disturbance during the tool-assembling process with force control. For a customized assembing tool, experiments on load parameter calibration and gravity compensation in non-contact condition are carried out. The experimental results show that the tool gravity compensation algorithm can obtain a high precision, meeting the requirements of local autonomous force control in tool-assembing task, while the maximum error of gravity compensation and gravity moment compensation are 1 N and 0.1 N·m, respectively.

Key words:　gravity compensation; force control; tool assembling; remote welding